ELSEVIER

Contents lists available at ScienceDirect

# Journal of Alloys and Compounds

journal homepage: www.elsevier.com/locate/jalcom





# Improvement of the strength of ternary eutectic V-Si-B alloys at ambient and high temperatures due to Cr additions

G. Hasemann a, \*, L. Thielemann a, W. Yang b, S. Ida c, R. Schwaiger b,d, K. Yoshimi c, M. Krüger a

- a Otto-von-Guericke University Magdeburg, Institute of Materials and Joining Technology, Universitätsplatz 2, Magdeburg 39106, Germany
- b Forschungszentrum Jülich GmbH, Institute of Energy and Climate Research, Structure and Function of Materials (IEK-2), Wilhelm-Johnen-Str, Jülich 52428, Germany
- <sup>c</sup> Tohoku University, Department of Materials Science, Graduate School of Engineering, 6-6-02 Aramaki Aza Aoba, Sendai, Miyagi 980-8579, Japan
- d RWTH Aachen University, Chair of Energy Engineering Materials, Faculty 5, Tempelgraben 55, Aachen 52056, Germany

#### ARTICLE INFO

Keywords: Vanadium-based alloys Compression test Deformation Intermetallics Yield strength

#### ABSTRACT

In the present study high-temperature compression tests on a chromium-alloyed ternary eutectic V-9Si-6.5B are reported. The ternary eutectic composition is located within the  $V_{SS}$  (V solid-solution)- $V_3Si-V_5SiB_2$  three-phase region of the respective V-rich corner of the phase diagram. The high-temperature compressive yield stresses were determined by the 0.5 % offset method and the plastic strain was obtained by subtracting the combined compliance of the testing machine and the specimen from the individually measured load-displacement curves. The microstructures in the as-cast and heat-treatment state (1400  $^{\circ}$ C / 100 hrs) were analyzed using SEM, EBSD and TEM observations. The effect of Cr on the ternary eutectic formation was studied. After compression testing, dislocation activities were observed in the  $V_{SS}$  and  $V_3Si$  phases, while the ternary intermetallic phases were dislocation-free. The high-temperature plasticity in the Cr-added ternary eutectic alloys V-9Si-6.5B+xCr is mainly governed the  $V_{SS}$  phase which forms the major phase of the eutectic. Thus, Cr additions are found to contribute to solid-solution strengthening in the ternary eutectic alloys while strongly influencing the deformability by decreasing the temperature at which brittle failure occurs in the present compression experiments.

#### 1. Introduction

Vanadium-silicide-based alloys for structural high-temperature applications have been studied in great detail over the last few years [1–4]. V-based alloys show great potential for fusion applications, due to their relatively low values of time to low-level waste (LLW) during neutron irradiation [5–7].

The baseline of the recent work on V-Si-B alloys has been laid by the Nowotny group [8] and the Nunes group [9–12] who mostly focused on close similarities between the well-studied Mo-Si-B system. However, recent studies of the V-Si-B alloy system have revealed new aspects of this ternary system, for example the discovery of a new phase composition, V<sub>8</sub>SiB<sub>4</sub>, after heat-treating alloys in the V<sub>SS</sub>-V<sub>3</sub>Si-V<sub>5</sub>SiB<sub>2</sub> phase field at 1400 °C [3]. Furthermore, a ternary eutectic reaction between the three phases V<sub>SS</sub>, V<sub>3</sub>Si and V<sub>5</sub>SiB<sub>2</sub> could be determined, in which the solid-solution phase forms the matrix [4].

In comparison to other refractory-based alloying systems, especially the Mo-Si-B system, vanadium shows some interesting advantages. First, vanadium has a much lower density which would make it suitable for high-temperature structural applications, i.e., as rotation parts in gas turbines. Second, if alloyed with silicon, molybdenum suffers from embrittlement, although its Si solubility is very low. Vanadium seems less sensitive to embrittlement after being alloyed with silicon – even at the maximum solubility of about 6.5 at% Si [2]. The  $V_{\rm SS}$ - $V_3$ Si- $V_5$ SiB $_2$  ternary eutectic, which is isomorphous to the Mo-Si-B system, may allow the fabrication of cast, forged or wrought components [7] due to the presence of the relatively ductile  $V_{\rm SS}$  major phase. One of the major drawbacks of V-based alloys might, however, be its poor oxidation resistance. Low alloyed  $V_{\rm SS}$  alloys [6,13–17] suffer from a very poor oxidation resistance at temperatures between 600 °C and 800 °C, which can be improved, but not entirely mitigated, by major additions of Ti, Cr, Al, Si and B [18–21].

Furthermore, alloys containing the  $V_{SS}$  phase as the major phase need to be strengthened to increase their high-temperature mechanical properties. The Perepezko group [22] investigated the influence of different alloying additions, including Ti, Zr, Hf, V, Nb, Ta, Cr, W, Re and Al, on the phase stability and microstructure constituency of various Mo-Si and Mo-Si-B phases. This general approach gives a basic

E-mail address: georg1.hasemann@ovgu.de (G. Hasemann).

<sup>\*</sup> Corresponding author.

understanding which alloying elements stabilize special phases in the Mo-Si portion of the ternary Mo-Si-B system. Since the V-Si-B system shows structural similarities to Mo-Si-B [8-12], some aspects of Perepezko's work might be useful for tailoring the compositions of V-Si-B alloys. Thus, alloying elements, such as Mo, Nb, Ta and W, may support the high-temperature resistance, strength and creep properties, while Ti, Cr and Al additions might be beneficial in terms of improving the oxidation resistance in addition to improving solid-solution hardening. Based upon these principle alloys design approaches [22], the present study is focused on different amounts of Cr-additions to the ternary-eutectic composition V-9Si-6.5B [4] to investigate the microstructure formation and the corresponding mechanical high-temperature compressive properties. Chromium has been chosen due to its high melting point ( $T_m = 1907$  °C), which is comparable to the melting point of vanadium (T  $_{m} = 1910~^{\circ}\text{C}$ ), and its stabilizing effect on the transition-metal-based (TM) A2 solid-solution phase, A15 and D81 phases, known as the  $TM_{SS}$ - $TM_3Si$ - $TM_5SiB_2$  phase field (TM = Mo, V) [22].

#### 2. Experimental procedures

The V-based alloys used in the present study were prepared via conventional arc-melting. Prior to melting, the alloy concentrations were carefully weighed in using high purity elemental chips or flakes of V (99.9 %), Si (99.99 %), B (99.0 %) and Cr (99.99 %). The molten buttons were flipped and re-melted five times to ensure good homogeneity. The weight loss after melting was  $\leq 1$ % indicating almost no changes from the nominal composition. The chemical alloy compositions were additionally verified by inductively coupled plasma optical emission spectroscopy (ICP-OES) and are summarized in Table 1. After melting, the buttons were cut and one half was wrapped in tantalum foil and heat-treated at 1400 °C for 100 hrs in flowing Ar atmosphere to reach thermodynamic equilibrium of the microstructures.

To investigate the solid-solution hardening effect, additional binary single-phase  $V_{SS}$  alloys V-(1–7.5 at%)Si and V-(5–30 at%)Cr were produced.

Samples for metallographic preparation were hot mounted in epoxy (Struers Poly Fast) and subsequently ground followed by a polishing finish with 3  $\mu m$  and 1  $\mu m$  diamond suspension and colloidal silica. The microstructural observations were carried out using a FEI Scios scanning electron microscope (SEM). The SEM images were typically obtained in the backscattered electron (BSE) mode. Electron backscatter diffraction (EBSD, Oxford Instruments) and X-ray diffraction (XRD, Bruker D8) were used for phase identification. Deformation was analyzed by means of local misorientation maps with a 3  $\times$  3 filter size. The maps display small orientation changes by calculating the average misorientation between every pixel and its surrounding pixels, thus highlighting regions of higher deformation. Misorientations above  $5^{\circ}$  are discarded in order to exclude abrupt orientation changes associated with grain boundaries. The resulting maps are color coded, where blue to red indicates misorientation angles of  $0^{\circ}$  to  $5^{\circ}$ .

EDS measurements, using a Zeiss Merlin (Zeiss Microscopy, Oberkochen, Germany) SEM equipped with a silicon drift detector (SDD, X-Max 150, Oxford instruments), were performed to measure the phase composition.

Thin specimens for investigation in a transmission electron

Table 1
Chemical analysis of as-cast V-Si-B+xCr alloys measured via ICP-OES.

Nominal composition	Si [at%]	B [at%]	Cr [at%]	V [at%]
V-9Si-6.5B	8.8	6.5	-	Bal.
V-9Si-6.5B-5Cr	8.8	6.2	4.9	Bal.
V-9Si-6.5B-10Cr	9.1	6.1	10.1	Bal.
V-9Si-6.5B-20Cr	8.5	5.9	20.2	Bal.
V-9Si-6.5B-30Cr	8.6	6.1	29.9	Bal.

microscope (TEM, Zeiss Libra 200 Cs) were prepared by focused ion beam milling (FIB, Zeiss Auriga). Images were recorded in the scanning transmission electron microscope (STEM) mode in order to avoid image artifacts caused by the bending of the thin specimen.

Cylindrical compression samples in the as-cast and heat-treated state having a typical length of 3 mm and a diameter of 1.8 mm were cut via electrical discharge machining (EDM). After cutting the samples were gently rolled on 800 and 1200 grit grinding paper to remove the burr left from EDM and to remove the EDM-damaged layer. The ground surface was finished by lapping using a suspension of glass bead blasting particles and ethanol and was stirred with a magnetic stirrer and an agitator for 8 hrs. The compression tests were performed at different temperatures using a Zwick/Roell Z100 electro-mechanical universal testing machine at a constant crosshead speed corresponding to an initial (engineering) strain rate of  $\dot{\varepsilon}=10^{-3}\,\mathrm{s}^{-1}$ . The compressive plastic strain was obtained by subtracting the combined compliance of the testing machine and the specimen from the individually measured load-displacement curves.

For the nanoindentation tests, the surfaces of the test samples were mechanically polished using 15 µm, 6 µm, 3 µm, and 1 µm diamond suspensions. The final polishing was conducted with colloidal silica for a duration of four hours. A nanoindenter G200X (KLA Instruments, Milpitas, CA, USA) equipped with a diamond Berkovich tip was used. The samples were indented at a constant indentation strain rate, i.e., the load *P* was increased as  $P/\dot{P} = 0.2 \text{ s}^{-1}$  until a maximum depth (*h*) of 200 nm was reached. After holding the maximum load constant for 5 s, the tip was unloaded within 10 s. The thermal drift rates were measured over 100 s after unloading to 7 % of the maximum load and the displacement was corrected accordingly. To obtain the hardness H and Young's modulus E of solid-solution phase in the heat-treated samples, three grids of  $5 \times 5$  indentations with a spacing of 5  $\mu$ m were performed on every sample. Because of the fine distribution of intermetallic phases in the solid-solution phases of the as-cast alloys, three grids of  $3 \times 3$  indentations with an indent spacing of 1.1 µm were performed for each of the as-cast samples. The Oliver-Pharr method [23] implemented using the open-source Python package micromechanics-indentationGUI [24] was used to determine hardness and Young's modulus assuming 0.07 and 1141 GPa for Poisson ratio (v) and Young's modulus of diamond, respectively, and for the Poisson ration of the solid-solution phase a value of 0.361 [25] was used.

## 3. Results and discussion

# 3.1. Cr-effect on the ternary eutectic V-Si-B microstructure

The microstructures of the V-Si-B+xCr alloys are shown in Fig. 1. Alloy V-9Si-6.5B represents the Cr-free ternary eutectic reference alloy for this work. As reported recently [4], the ternary eutectic reaction is located within the  $V_{SS}$ -V $_{3}$ Si-V $_{5}$ SiB $_{2}$  phase field with the respective volume phase fractions of about 65 %  $V_{SS}$ , 20 %  $V_{3}$ Si and 15 %  $V_{5}$ SiB $_{2}$  measured via EBSD. After the heat treatment, the microstructure coarsens and the  $V_{5}$ SiB $_{2}$  phase transforms into the  $V_{8}$ SiB $_{4}$  phase, which has, based on our current understanding, the same space group as  $V_{5}$ SiB $_{2}$  (I4/mcm, No. 140) but with a c-axis increased by a factor of 1.56 [3]. The volume fraction of phases changed accordingly to about 55 %  $V_{SS}$ , 25 %  $V_{3}$ Si and 20 %  $V_{8}$ SiB $_{4}$ .

By subsequently adding 5, 10, 20 and 30 at% Cr to the alloy V-9Si-6.5B, the as-cast microstructure does not change leading to the conclusion, that chromium has no significant influence on the ternary eutectic solidification. This might be attributed to comparable melting points and atomic radii of V ( $T_m = 1910\,^{\circ}\text{C}$  [26],  $r_V = 132\,\text{pm}$  [27]) and Cr ( $T_m = 1907\,^{\circ}\text{C}$  [28],  $r_{Cr} = 125\,\text{pm}$  [27]). Exemplary for all as-cast compositions EBSD images are shown for alloys containing 20 and 30 at% Cr in Fig. 1, highlighting no microstructural changes in the cast conditions. Same observations could be made by just using BSE imaging for the

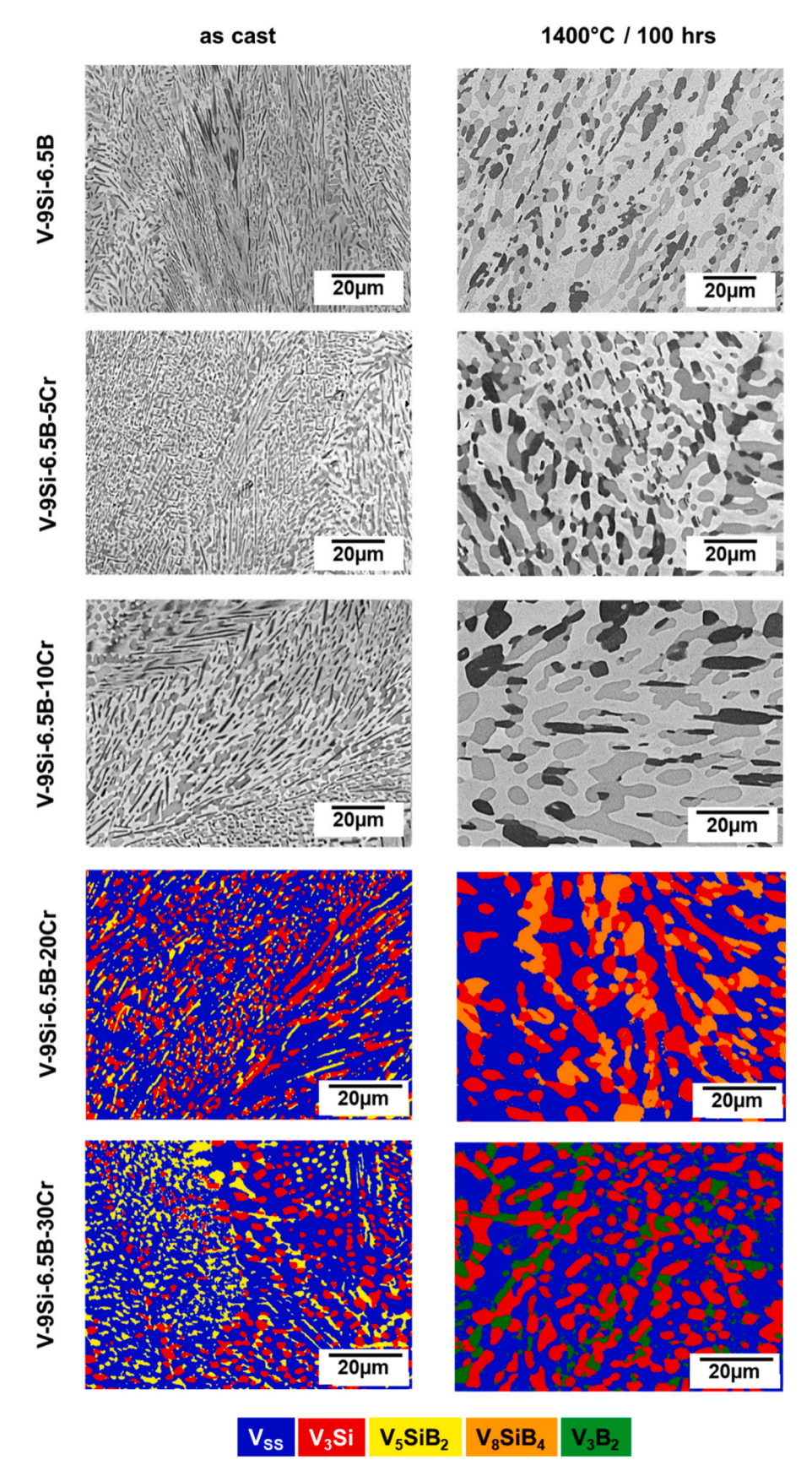


Fig. 1. SEM-BSE and EBSD images of the as-cast and heat-treated ternary eutectic V-Si-B+xCr alloys.

heat-treated conditions, where all microstructures would appear almost identically. However, EBSD revealed interesting differences. First of all, Cr additions of 5–20 at% also lead to the formation of the new phase  $V_8SiB_4$  which involves Cr-substitutions on the V-sites, while the volume phase fractions are comparable to the Cr-free alloy. Interestingly, additions of 30 at% Cr seem to stabilize a new three-phase field consisting of the  $V_{SS}$ ,  $V_3Si$  and  $V_3B_2$  phase.

Table 2 correlates the chemical phase composition measured via EDS with the respective Cr additions comparing the as-cast and heat-treated state of all alloys investigated here. For the as-cast condition, the Si concentration within the  $V_{SS}$  and  $V_3S$ i phases stays relatively constant, while the Cr content steadily increases in both phases. Both phases have a negligible B solubility [11]. By contrast, the Si concentration in the  $V_5SiB_2$  phase decreases, while B and Cr show higher concentrations the more Cr is added to the alloy.

In general, the heat-treated condition follows similar trends: The silicon concentration in the  $V_{SS}$  and  $V_3S$ i phases remains constant, while, in case of the  $V_{SS}$  phase, on a lower level than in the as-cast state. This can be attributed to lower solubility values of Si in the  $V_{SS}$  phase at 1400 °C [26]. The Cr concentration in both phases also increases with increasing Cr addition to the alloys investigated and are, within the range of experimental scatter, comparable to the as-cast conditions. The most obvious change refers to the solid-state transformation of  $V_5SiB_2$  to  $V_8SiB_4$  during heat treatment. As the Cr concentration in the alloys increases, the Cr solubility in  $V_8SiB_4$  also increases, while the Si and B concentrations remain unaffected. An exception must be made for the high Cr-containing alloy V-9Si-6.5B-30Cr, where the  $V_3B_2$  phase is formed after heat treatment, in which a negligible Si solubility is reported [11] and measured.

As a result of the microstructural and chemical analyses, it can be noted that Cr can be solved in all three eutectic phases as proposed by the alloy strategy of Sakidja and Perepezko [22]. The formation of the new phase  $V_8SiB_4$  is not affected by Cr additions, except for the alloy containing 30 at% Cr, where the  $V_3B_2$  phase has formed during heat-treatment at 1400 °C.

The lattice parameters of the individual phases were additionally determined via XRD and are summarized in Table 3. Considering the experimental scatter, the Si concentration in  $V_{SS}$  and  $V_3Si$  can be taken

**Table 2**EDS phase composition (given in at%) in dependence of the individual Cr additions compared in the as-cast and heat-treated conditions.

		V-9Si- 6.5B	V-9Si- 6.5B-5Cr	V-9Si- 6.5B-10Cr	V-9Si- 6.5B-20Cr	V-9Si- 6.5B-30Cr	
			a	s-cast			
V <sub>SS</sub>	Si	5.5	4.9	5.7	5.1	5.0	
	В	-	-	-	-	-	
	Cr	-	6.6	12.9	25.8	42.2	
V <sub>3</sub> Si	Si	18.3	18.4	18.7	18.6	17.5	
	В	-	-	-	-	-	
	Cr	-	4.2	8.5	17.5	32.2	
$V_5SiB_2$	Si	9.9	8.0	8.7	7.6	5.5	
	В	24.8	26.4	26.7	29.3	31.2	
	Cr	-	2.4	4.2	8.8	16.9	
			heat-treated at	1400 °C / 100	hrs		
V <sub>SS</sub>	V <sub>SS</sub> Si 3.4		3.7	3.8	3.5	3.7	
В	-	-	-	-	-		
	Cr	-	6.8	13.4	31.2	43.7	
V <sub>3</sub> Si	Si	18.8	18.6	19.0	18.3	18.3	
	В	-	-	-	-	-	
	Cr -	4.5	7.9	21.6	30.7		
V <sub>8</sub> SiB <sub>4</sub>	Si	6.5	6.4	6.2	5.9	-	
	В 30.7		31.4	32.3	31.9	-	
	Cr	-	1.6	3.0	8.6	-	
$V_3B_2$	Si	-	-	-	-	0.2	
	В	-	-	-	-	39.7	
	Cr	-	-	-	-	12.9	

as constant (Table 2), the lattice parameters of both phases decreases with increasing Cr additions for the as-cast as well as for the heat-treated state, as expected for Cr atoms partially occupying V-sites. The same is observed for the ternary phases  $V_5 {\rm SiB}_2$  and  $V_8 {\rm SiB}_4$ .

# 3.2. Temperature-dependent mechanical properties of ternary eutectic V-Si-B-xCr alloys

Recently, compressive plastic deformability at room temperature was reported on a hypoeutectic alloy V-9Si-5B [2], which motivated our study of the temperature dependent compression properties of pure eutectic V-Si-B alloys and their modification with Cr additions. Fig. 2 exemplifies the behavior of the ternary eutectic alloy V-9Si-6.5B and its modifications containing 20 at% Cr in their as-cast and heat-treated conditions. These compressive stress-strain curves are representative for all alloys investigated and the plateau-like stress behavior at strains higher the 5 % is attributed to shear plastic deformation. The shear plastic behavior makes it difficult to distinguish the onset of plastic deformation. The V<sub>SS</sub> phase seems to exhibit only modest work hardening [29], thus, the flow criterion is first fulfilled in a small volume fraction of the sample. This results in a change in the stress-strain slope before the actual maximum compression (yield) strength is reached, at which the stress is high enough to cause macroscopic shear plasticity at a constant stress level. Due to the modest work hardening rate, plasticity is localized in the shear zone.

The Cr-free eutectic base alloy V-9Si-6.5B shows deformability at room temperature, which is attributed to the ductile V<sub>SS</sub> major phase of the ternary eutectic microstructure [2]. Si acts as a strong solid-solution strengthener in vanadium. In contrast to the Moss [30], even high Si concentrations of about 5.5 at% Si (the maximum solubility is reached at about 6.5-7 at% Si [2,26]) did not lead to embrittlement. Additions of Cr subsequently increase the compressive strength of the alloys as shown for 20 at% Cr in Fig. 2. However, alloying with chromium leads to embrittlement of the alloys and thus, increases the BDTT, such that compression testing at temperatures lower than 600 °C causes direct brittle failure. As shown in Table 2, Cr solves in each phase of the as-cast or heat-treated alloys. The increased compressive yield stress with increasing Cr concentrations of the alloys can be attributed to mainly solid-solution strengthening with Cr – not only within the V<sub>SS</sub> phase, but also of the intermetallic phases. Fig. 3 illustrates the linear correlation of either Si or Cr additions in the vanadium solid-solution phase and the corresponding yield stress at room temperature to assume the hardening contribution of both elements to the V<sub>SS</sub> eutectic major phase.

The effect of Si and Cr on solid-solution strengthening was further investigated and evaluated by nanoindentation tests on the  $V_{SS}$  phase of the V-9Si-6.5B+xCr alloys at room temperature. In Fig. 4 the Si and Cr concentrations measured for the  $V_{SS}$  phase, Table 2, were plotted against the overall Cr additions to the ternary eutectic alloy V-9Si-6.5B and plotted in comparison to the indentation hardness H and Young's modulus E. Independent of the alloy's condition (as-cast or heat-treated at 1400 °C for 100 hrs), the hardness increased with increasing Cr concentrations added to the eutectic base alloy indicating the additional strengthening effect of Cr, while the Si concentration remained almost constant. Hence, the increase in nanoindentation hardness (strength) can directly by attributed to the Cr additions leading to further strengthening of the eutectic  $V_{SS}$  major phase.

The results of the compression test of all alloys investigated in this study are summarized in Fig. 5a) showing the temperature-dependent compressive yield stress of the V-9Si-6.5B-xCr alloys. As already mentioned, subsequently adding Cr to the ternary eutectic base alloy V-9Si-6.5B increases the compressive strength. As directly compared to the as-cast condition, the heat treatment at 1400 °C for 100 hrs leads to slightly lower  $\sigma_{0.5}$  values which is attributed to the lower Si solubility in the VSS phase leading to solid-solution softening of the eutectic's major phase, while the Cr concentration remains unaffected by the heat treatment (Table 2). It has to be mentioned that the role and

**Table 3**Measured lattice parameters of V-Si-B+xCr alloys.

		Lattice parameter [Å]							
		V <sub>SS</sub> a	V <sub>3</sub> Si a	V <sub>5</sub> SiB <sub>2</sub> a	V <sub>5</sub> SiB <sub>2</sub> c	V <sub>8</sub> SiB <sub>4</sub> a	V <sub>8</sub> SiB <sub>4</sub> c	V <sub>3</sub> B <sub>2</sub> a	V <sub>3</sub> B <sub>2</sub> c
as-cast	V-9Si-6.5B	3.022	4.744	5.773	10.743	-	-	-	-
	V-9Si-6.5B-5Cr	3.017	4.734	5.763	10.732	-	-	-	-
	V-9Si-6.5B-10Cr	3.007	4.722	5.751	10.714	-	-	-	-
	V-9Si-6.5B-20Cr	2.985	4.702	5.714	10.699	-	-	-	-
	V-9Si-6.5B-30Cr	2.966	4.680	5.725	10.831	-	-	-	-
1400 °C / 100 hrs	V-9Si-6.5B	3.025	4.741	-	-	5.767	16.795	-	-
	V-9Si-6.5B-5Cr	3.020	4.731	-	-	5.761	16.789	-	-
	V-9Si-6.5B-10Cr	3.013	4.722	-	-	5.754	16.771	-	-
	V-9Si-6.5B-20Cr	2.990	4.701	-	-	5.738	16.734	-	-
	V-9Si-6.5B-30Cr	2.962	4.680	-	-	-	-	5.700	3.019

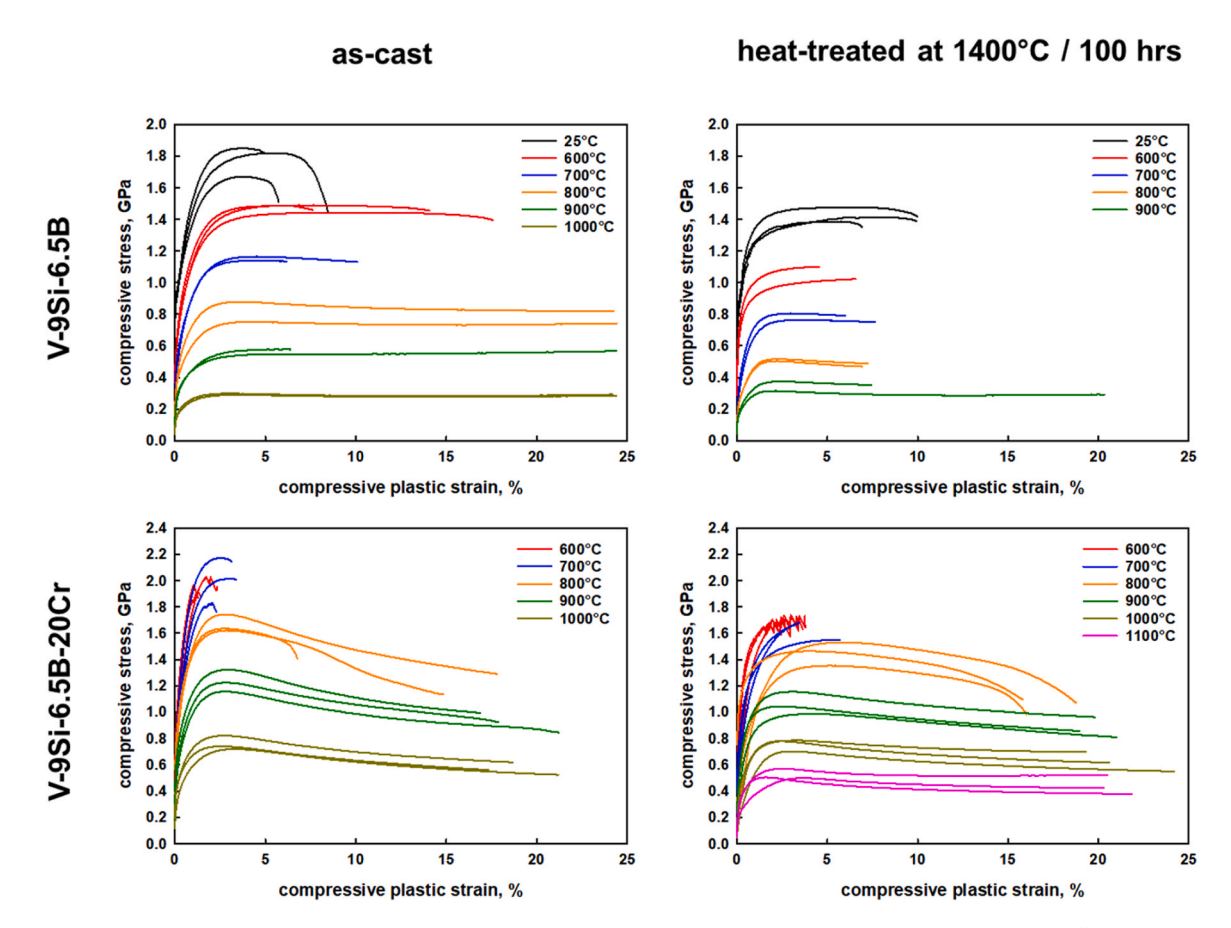


Fig. 2. Typical compressive stress vs. plastic strain curves as a function of test temperature for the Cr-free ternary eutectic base alloys V-9Si-6.5B and V-9Si-6.5B-20Cr.

contribution to strength of the new phase  $V_8SiB_4$  is not yet clear and will be further investigated. Interestingly, the heat-treated alloy V-9Si-6.5B-30Cr tends to show almost no softening compared to its as-cast state, even though the chemical compositions of the  $V_{SS}$  and  $V_3Si$  phases are comparable to the other heat-treated alloys having lower Cr concentrations (Table 2).

Fig. 5b) compares the heat-treated, homogenized V-9Si-6.5B-xCr alloys to literature values of the V-4Cr-4Ti [6] solid-solution alloy being discussed for fusion applications as well as to a state-of-the-art  $\gamma$ -TiAl [31] and Ni-based alloys [32,33]. Please note that data for V-4Cr-4Ti and TNB-V2 were obtained under tensile loading, due to the lack of compressive data of published literature. Thus, even if the data suggest same or superior properties as compared to the strength of the  $\gamma$ -TiAl alloy TNB-V2, it is (in fact) unlikely that the compressive strength will yield the same magnitude as for the tensile strength – even as noted

before, that brittle fracture occurs at compressive test temperatures below 600 °C. By alloying with Cr of about 10–20 at%, however, comparable compressive strength values of Ni-based superalloys can be reached. Besides the tensile properties, creep resistance and oxidation performance of the newly designed V-Si-B+xCr alloys will be crucial points for further alloy development. It might be interesting to see, if V-Si-B+Cr alloys may bridge the gap between TiAl and Ni-based superalloys for high-temperature turbine applications in future. Seeking for new high-temperature materials for turbine applications may just be one driving force for the development of V-Si-B alloys since V-Si-B alloys may become in interesting material for fusion applications in future, due to the relatively low values of time to LLW during neutron irradiation.

The compressive deformation mechanism of the ternary eutectic V-Si-B and V-Si-B+xCr alloys is mainly governed by deformation of the  $V_{\rm SS}$  phase. Observations of local misorientation maps obtained from EBSD

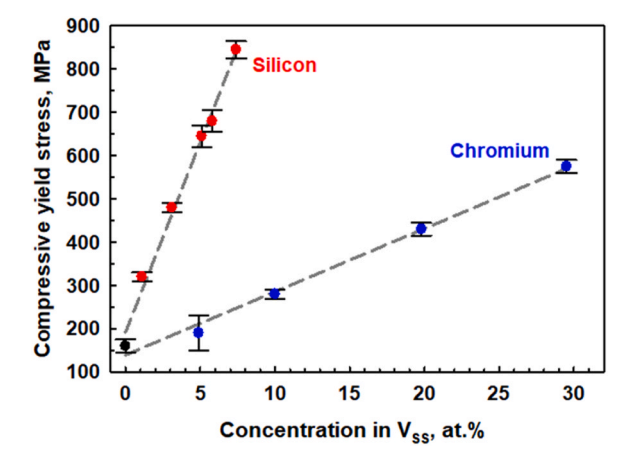
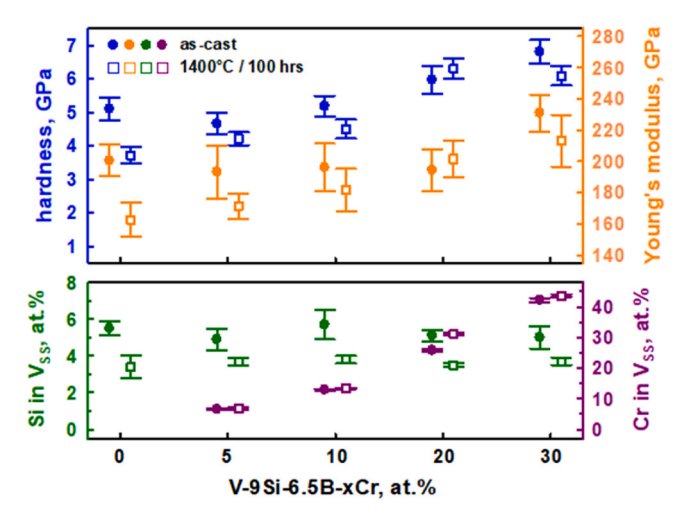


Fig. 3. Si and Cr contribution to the yield strength of the corresponding binary  $V_{SS}$  phases at room temperature. Both curves were fitted to pure vanadium at 0 at% Si and Cr.



**Fig. 4.** Hardness and Young's modulus determined from nanoindentation experiments as a function of the Cr content in the alloys. The corresponding Si and Cr concentrations in the  $V_{SS}$  eutectic major phase (lower graph) demonstrate the strengthening effect of both alloying elements.

measurements confirm the recently obtained results [2] that plasticity is mostly observed in the  $V_{SS}$  phase and high stress concentrations occur at the  $V_{SS}\text{-}V_3Si$ ,  $V_{SS}\text{-}V_5SiB_2$  and  $V_{SS}\text{-}V_8SiB_4$  interfaces. Local misorientation maps obtained from samples tested at 800 °C and 1000 °C further suggest additional plasticity of the  $V_3Si$  phase, which was confirmed by STEM observations (Fig. 6). The coupled EBSD and STEM investigations show high stress intensities at the phase boundaries with dislocation networks and pile-ups clearly visible at  $V_{SS}\text{-}V_3Si$  interfaces. Furthermore, dislocations can be seen in the  $V_3Si$  phase, piling-up at  $V_{SS}\text{-}V_3Si$  and  $V_3Si\text{-}V_5SiB_2$  interphases, especially in samples deformed at 800 °C and 1000 °C.

#### 4. Summary and conclusions

It was shown that ternary eutectic V-Si-B alloys are potential candidates as light-weight materials for structural applications at high temperatures. However, the V solid-solution major phase of the eutectic needs to be strengthened to fulfill the high demands of applications, such as high-temperature strength, creep and oxidation resistance. The present work introduces Cr as an effective alloying element for V-Si-B alloys to reach these goals. The present study on the chromium effect to the ternary eutectic V-Si-B alloy composition can be summarized as follows:

- The ternary eutectic composition at V-9Si-6.5B featuring the ductile  $V_{SS}$  as the major phase. Cr additions between 5 and 30 at% do not affect the eutectic formation and stabilize the eutectic phases  $V_{SS}$ ,  $V_3Si$  and  $V_5SiB_2$ .
- Cr acts as effective solid-solution strengthener and can be solved in each phase but leads to embrittlement and thus, resulting in brittle failure during the present compression test at temperatures < 600 °C.</li>
- Nanoindentation experiments conducted on the V<sub>SS</sub> phase demonstrated the effect of Cr on solid-solution strengthening and helps to interpret the compression tests conducted on ternary eutectic V-Si-B+xCr alloys and the contribution of Cr to the macroscopic stress-strain behavior.
- $\bullet$  The heat treatment at 1400 °C does not affect the solid-state transformation from  $V_5SiB_2$  into  $V_8SiB_4$  at Cr additions <30 at%. At 30 at %, however, Cr seems to promote the  $V_3B_2$  formation instead of  $V_8SiB_4$  forming the  $V_{SS}\text{-}V_3Si\text{-}V_3B_2$  phase field after annealing at 1400 °C for 100 hrs.
- $\bullet$  While deformation is mostly attributed to occur in the  $V_{SS}$  phase, using STEM observations of deformed samples, dislocations were also found to start operating in  $V_3Si$  at test temperatures of 800  $^\circ C.$

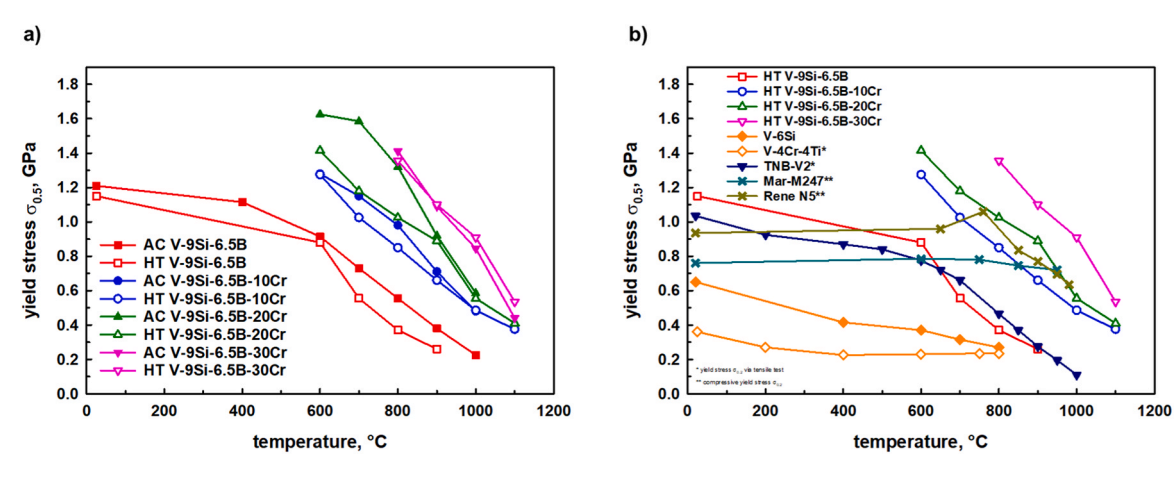


Fig. 5. Comparison of the compressive yield strength as a function of temperature, a) between the as-cast (AC) and heat-treated (HT) ternary eutectic V-Si-B+xCr alloys and b) the heat-treated alloy of the present work with available literature values of V-4Cr-4Ti [6], the  $\gamma$ -TiAl TNB-V2 (Ti-45Al-8 Nb-0.2C NL) [31] and Mar-M247 and Rene N5 Ni-based superalloys [32,33].

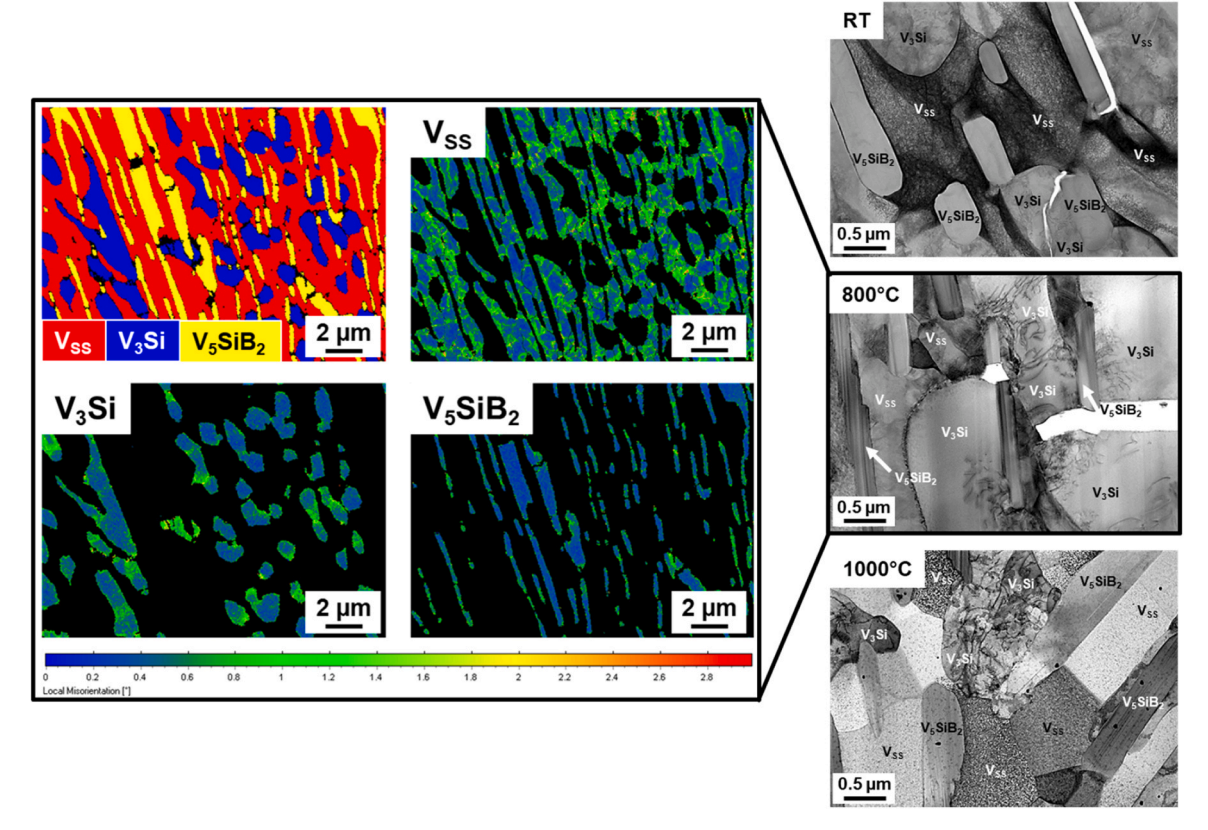


Fig. 6. Ternary eutectic alloy V-9Si-6.5B after compressive deformation at different test temperatures. Local misorientation maps, exemplarily shown for samples deformed at 800 °C, indicating plastic behavior in the  $V_{SS}$  and  $V_3Si$  phase and high stress intensities at phase boundaries particularly at  $V_{SS}$ - $V_5SiB_2$  and  $V_3Si-V_5SiB_2$  interfaces. STEM bright field image revealed no dislocation activities in the intermetallic phases at room temperature (RT). As in the heavily deformed  $V_{SS}$ , dislocations can clearly be observed in  $V_3Si$  at both high temperatures but not within the  $V_5SiB_2$  phase.

 The annealing treatment slightly decreases the compressive yield strength and shows comparable compression strength as compared to the state-of-the-art Ni-based alloys. Thus, Cr-added ternary eutectic V-Si-B alloys are potentially interesting candidates for lightweight high-temperature applications.

#### **Declaration of Competing Interest**

The authors declare that they have no known competing financial interests or personal relationships that could have appeared to influence the work reported in this paper.

# Data availability

Data will be made available on request.

# Acknowledgements

The study was funded by the German Research Foundation (DFG) under the grant numbers 410338871 (HA 8534/3–1) and 432703793 (HA 8534/4–1). Financial support of the Methodisch-Diagnostisches Zentrum Werkstoffprüfung (MDZWP) e.V., Magdeburg, Germany is greatly acknowledged. We kindly thank C. Müller (OVGU) for providing data of the single-phase V-Cr solid-solutions, U. Betke (OVGU) for supporting the XRD measurements, Dr. E. Wessel (IEK-2, FZ Jülich) and Dr. D. Grüner (IEK-2, FZ Jülich) for their assistance in EDS measurements and STEM investigation and D. Eßer (IEK-2, FZ Jülich) for the FIB operation.

## References

- G. Hasemann, Experimental Study of the Liquidus Surface in the V-rich Portion of the V-Si-B System (submitted), J. Alloy. Compd. (2019) (submitted).
- [2] G. Hasemann, C. Müller, D. Grüner, E. Wessel, M. Krüger, Room temperature plastic deformability in V-rich V-Si-B alloys, Acta Mater. 175 (2019) 140–147, https://doi.org/10.1016/j.actamat.2019.06.007.
- [3] W.G. Yang, R.S. Touzani, G. Hasemann, M. Yazlak, M. Ziegner, B. Gorr, R. Schwaiger, M. Krüger, V8SiB4 — A new ternary phase in the V–Si–B system, Intermetallics 151 (2022) 107691, https://doi.org/10.1016/j. intermet.2022.107691.
- [4] W.G. Yang, G. Hasemann, M. Yazlak, B. Gorr, R. Schwaiger, M. Krüger, Ternary Vss-V3Si-V5SiB2 eutectic formation in the V-Si-B system, J. Alloy. Compd. 902 (2022) 163722, https://doi.org/10.1016/j.jallcom.2022.163722.
- [5] M.R. Gilbert, T. Eade, T. Rey, R. Vale, C. Bachmann, U. Fischer, N.P. Taylor, Waste implications from minor impurities in European DEMO materials, Nucl. Fusion. 59 (2019), https://doi.org/10.1088/1741-4326/ab154e.
- [6] S.J. Zinkle, H. Matsui, D.L. Smith, A.F. Rowcliffe, E.V. van Osch, K. Abe, V. A. Kazakov, Research and development on vanadium alloys for fusion applications, J. Nucl. Mater. 258–263 (1998) 205–214, https://doi.org/10.1016/S0022-3115 (98)00269-4.
- [7] T. Muroga, T. Nagasaka, K. Abe, V.M. Chernov, H. Matsui, D.L. Smith, Z.Y. Xu, S. J. Zinkle, Vanadium alloys overview and recent results, J. Nucl. Mater. 307–311 (2002) 547–554, https://doi.org/10.1016/S0022-3115(02)01253-9.
- [8] H. Kudielka, H. Nowotny, G. Findeisen, Untersuchungen in den systemen: V-B, Nb-B, V-Si-B und Ta-B-Si, Mh. Chem. 88 (1957) 1048–1055.
- [9] B.B. De Lima, C.A. Nunes, G.C. Coelho, P.A. Suzuki, P. Rogl, Evaluation of the invariant reactions of the V-B system, J. Phase Equilibria Diffus. 25 (2004) 134–139, https://doi.org/10.1361/15477030418541.
- [10] B.B. De Lima-Kühn, A.A.A.P. Da Silva, A.P. Suzuki, G.C. Coelho, C.A. Nunes, Microstructural characterization of as-cast V-Si alloys and reevaluation of the invariant reactions involving the liquid phase of the V-Si system, Mater. Res. 19 (2016) 1122–1126.
- [11] C.A. Nunes, B.B. De Lima, G.C. Coelho, P.A. Suzuki, Isothermal Section of the V-Si-B System at 1600°C in the V-VSi2-VB Region, J. Phase Equilibria Diffus. 30 (2009) 345–350, https://doi.org/10.1007/s11669-009-9533-y.
- [12] A.A.A.P. Da Silva, N. Chaia, F. Ferreira, G. Carvalho Coelho, J.M. Fiorani, N. David, M. Vilasi, C.A. Nunes, Thermodynamic modeling of the V-Si-B system, Calphad Comput. Coupling Phase Diagr. Thermochem. 59 (2017) 199–206, https://doi.org/10.1016/j.calphad.2017.10.001.

- [13] M. Satou, K. Abe, H. Kayano, High-temperature deformation of modified V-Ti-Cr-Si type alloys, J. Nucl. Mater. 179–181 (1991) 757–761, https://doi.org/10.1016/ 0022-3115(91)90199-H.
- [14] K. Sakai, M. Satou, M. Fujiwara, K. Takanashi, A. Hasegawa, K. Abe, Mechanical properties and microstructures of high-chromium V-Cr-Ti type alloys, J. Nucl. Mater. 329–333 (2004) 457–461, https://doi.org/10.1016/j. inucmat.2004.04.089.
- [15] M.C. Cai, J.T. Zhang, L.S. Niu, H.J. Shi, Strain-rate sensitivity and fracture mode of V-5Cr-5Ti alloy, Scr. Mater. 62 (2010) 524–527, https://doi.org/10.1016/j. scriptamat.2009.12.035.
- [16] Z.D. Li, Q. Li, Y. Li, C.G. Lin, S. Cui, T.D. Ma, Mechanical properties and precipitation evolution behavior of V-5Cr-5Ti alloy after cold rolling, Fusion Eng. Des. 114 (2017) 76–83, https://doi.org/10.1016/j.fusengdes.2016.11.017.
- [17] Z.D. Li, Q. Li, Y. Li, T.D. Ma, Microstructure and properties of V-5Cr-5Ti alloy after hot forging, Fusion Eng. Des. 127 (2018) 83–90, https://doi.org/10.1016/j. fusenades 2017 12 029
- [18] J. Williams, M. Akinc, Oxidation behavior of V5Si3 based materials, Intermetallics 6 (1998) 269–275, https://doi.org/10.1016/S0966-9795(97)00081-2.
- [19] K. Natesan, M. Uz, Oxidation performance of V-Cr-Ti alloys, Fusion Eng. Des. 51–52 (2000) 145–152, https://doi.org/10.1016/S0920-3796(00)00308-2.
- [20] J.M. Chen, T. Muroga, S.Y. Qiu, T. Nagasaka, W.G. Huang, M.J. Tu, Y. Chen, Y. Xu, Z.Y. Xu, The development of advanced vanadium alloys for fusion applications, J. Nucl. Mater. 329–333 (2004) 401–405, https://doi.org/10.1016/j.inucmat 2004 04 080
- [21] N. Chaia, S. Mathieu, T. Cozzika, F. Rouillard, C. Desgranges, J.L. Courouau, C. Petitjean, N. David, M. Vilasi, An overview of the oxidation performance of silicide diffusion coatings for vanadium-based alloys for generation IV reactors, Corros. Sci. 66 (2013) 285–291, https://doi.org/10.1016/j.corsci.2012.09.031.
- [22] R. Sakidja, J.H. Perepezko, S. Kim, N. Sekido, Phase stability and structural defects in high-temperature Mo-Si-B alloys, Acta Mater. 56 (2008) 5223–5244, https://doi.org/10.1016/j.actamat.2008.07.015.

- [23] W.C. Oliver, G.M. Pharr, An improved technique for determining hardness and elastic modulus using load and displacement sensing indentation experiments, J. Mater. Res. 7 (1992) 1564–1583, https://doi.org/10.1557/JMR.1992.1564.
- [24] W. Yang, S. Brinckmann, R. Schwaiger, micromechanics/indentationGUI: v0.1.26, (2024). https://doi.org/https://doi.org/(10.5281/zenodo.11563150).
- [25] D.I. Bolef, R.E. Smith, J.G. Miller, Elastic properties of vanadium. I. Temperature dependence of the elastic constants and the thermal expansion, Phys. Rev. B. 3 (1971) 4100–4108, https://doi.org/10.1103/PhysRevB.3.4100.
- [26] J.F. Smith, The Si-V (Silicon-Vanadium) System, Bull. Alloy Phase Diagr. 2 (1981) 42–48.
- [27] W.D. Callister, D.G. Rethwisch. Materials Science and Engineering, Ninth Ed., John Wiley & Sons, Inc, 2015.
- [28] H. Okamoto, Cr-Si (Chromium-Silicon), –593, J. Phase Equilibria. 22 (2001) 593, https://doi.org/10.1361/105497101770332866.
- [29] K. Fukumoto, T. Onitsuka, M. Narui, Dose dependence of irradiation hardening of neutron irradiated vanadium alloys by using temperature control rig in JMTR, Nucl. Mater. Energy 9 (2016) 441–446, https://doi.org/10.1016/j. nme.2016.03.010.
- [30] D. Sturm, M. Heilmaier, J.H. Schneibel, P. Jéhanno, B. Skrotzki, H. Saage, The influence of silicon on the strength and fracture toughness of molybdenum, Mater. Sci. Eng. A. 463 (2007) 107–114, https://doi.org/10.1016/j.msea.2006.07.153.
- [31] J.-P. Monchoux, A. Couret, L. Durand, T. Voisin, Z. Trzaska, M. Thomas, Elaboration of metallic materials by SPS: processing, microstructures, properties, and shaping, Met. (Basel) 11 (2021) 322, https://doi.org/10.3390/met11020322.
- [32] A.M.S. Costa, J.P. Oliveira, V.F. Pereira, C.A. Nunes, A.J. Ramirez, A. P. Tschiptschin, Ni-based Mar-M247 superalloy as a friction stir processing tool, J. Mater. Process. Technol. 262 (2018) 605–614, https://doi.org/10.1016/j. imatprotec.2018.07.034.
- [33] Z. Shang, X. Wei, D. Song, J. Zou, S. Liang, G. Liu, L. Nie, X. Gong, Microstructure and mechanical properties of a new nickel-based single crystal superalloy, J. Mater. Res. Technol. 9 (2020) 11641–11649, https://doi.org/10.1016/j. jmrt.2020.08.032.